Supercond. Sci. Technol. **24** (2011) 095007 (5pp) doi:10.1088/0953-2048/24/9/095007

Superconductivity in $Th_3Ni_5C_5$

A J S Machado[1,2], T Grant[1] and Z Fisk[1]

[1] Escola de Engenharia de Lorena, Universidade de São Paulo, PO Box 116, Lorena, SP, Brazil
[2] Departments of Physics and Astronomy, University of California at Irvine, Irvine, CA 92697, USA

Received 25 April 2011, in final form 30 June 2011
Published 28 July 2011
Online at stacks.iop.org/SUST/24/095007

Abstract
The existence of a new metallic carbide of composition $Th_3Ni_5C_5$ was reported in the literature in 1991. This compound is a new orthorhombic prototype structure. In this work we report a reinvestigation of the synthesis of this material and we find that the $Th_3Ni_5C_5$ compound is a new bulk superconducting material. Despite the high concentration of Ni in this compound, we find bulk superconductivity with superconducting critical temperature of $T_c = 5.0$ K and an upper critical field of $\mu_o H_{c2} = 5.8$ T. Details of the superconducting state with specific heat, magnetization, and resistivity measurements are discussed.

(Some figures in this article are in colour only in the electronic version)

1. Introduction

Binary metal carbides have long been known to exist. Often the structures are binary composed of two elements carbon and T, RE, or A, where T designates a transition metal, RE a rare-earth metal, and A an alkaline-earth metal. The carbon–carbon bond is a way of classifying these materials. CaC_2 [1] or UC_2 [2], ThC_2 [3] and Pu_2C_3 [4] type structures belong to the first class. A common feature of this structure type is that there are distinct, strongly bonded C_2 pairs isolated from each other in the structures. The short contact between dimer and metal atoms also gives rise to strong metal–carbon interactions. Many members of this family exhibit interesting electric and magnetic properties [5–10]. Ternary carbides have also been receiving great attention, due to their potential importance in nuclear technology and in making permanent magnets. For example, many investigations on conductivity and magnetic properties have been made on $R_2Fe_{14}C$ systems (R = Gd, Dy, Er, and Lu) [11, 12]. It has been reported that Er_2FeC_4 is paramagnetic at room temperature and Y_2FeC_4 becomes superconducting at $T_c \sim 3.6$ K [13]. Like binary systems the ternary carbides can be classified into categories containing bonded carbon pairs and those containing isolated C atoms [14, 15]. Solid state ternary transition metal carbides containing carbon, a transition metal, and a highly electropositive multivalent metal such as (Ln), Sc, Y, or Th, exhibit a number of structural features resembling those in metal carbonyls and other transition metal derivatives of π-acceptor hydrocarbon ligands. The complete ionization of the electropositive metal to the stable ions Ln^{3+}, Y^{3+}, or Th^{4+} leads to a negatively charged transition metal–carbon subnetwork, which may be considered to be an organometallic net. Using this description, these compounds can be seen as negatively charged organometallic polymers embedded in a matrix of positive ions [16]. In many of these ternary compounds the transition metal atom can be assigned a low formal oxidation state reminiscent of the metal oxidation state in metal carbonyls and metal–olefin complexes. Indeed, many of the ternary transition metal carbides contain C_2 structural units with carbon–carbon distance inside 1.32–1.47 Å intervals, suggestive of carbon–carbon double bonds. These structural units may be regarded as being derived from C_2^{4-} anions obtained by the complete deprotonation of ethylene. To our knowledge the first nickel-based ternary carbide superconductor is the $LaNiC_2$ compound, which exhibits a superconducting critical temperature close to 2.7 K [17].

Moss [18] reported the discovery of the two new compounds Th_2NiC_2 and $Th_3Ni_5C_5$. $Th_3Ni_5C_5$ crystallizes with a new orthorhombic structure type (space group $Cmcm$) with the lattice constants $a = 13.92$ Å, $b = 7.14$ Å, and $c = 7.04$ Å, and $Z = 4$, where Z means the number of chemical formula per unit cell. $Th_3Ni_5C_5$ compound contains two-dimensionally infinite nickel–carbon sheets, while in Th_2NiC_2 the NiC_2 units are separated from each other. $Th_3Ni_5C_5$ contains two C_2 pairs per formula unit, with carbon–carbon distance of about 1.37 Å. The Th_2NiC_2 compound crystallizes in the tetragonal symmetry with space group $I4/mmm$ and prototype structure Na_2HgO_2, with lattice parameters $a = 3.75$ Å and $c = 12.35$ Å. In Moss's paper the author concluded that both compounds are Pauli paramagnetic. However, in this work we find that $Th_3Ni_5C_5$ is a bulk superconductor,

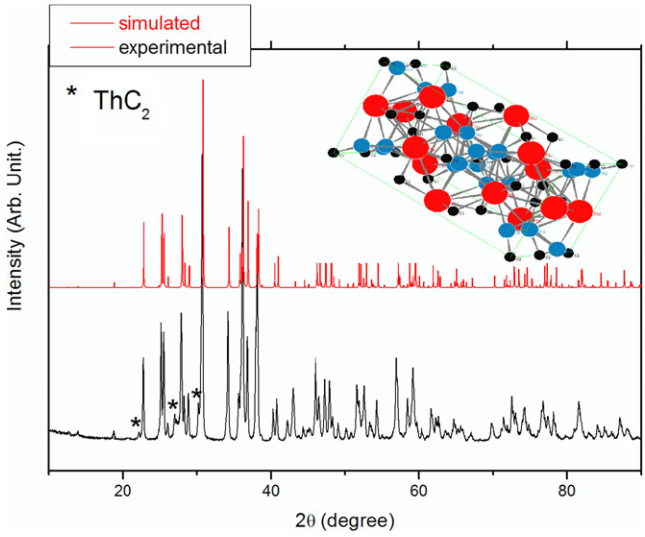

Figure 1. Comparison between the experimental (black line) and simulated (red line) diffraction patterns, showing good agreement between experiment and simulation. The minority impurity of ThC_2 is represented by the * symbol. The inset shows a schematic unit cell where red spheres represent Th atoms, blue represent Ni atoms, and black spheres represent carbon atoms.

with superconducting critical temperature close to 5.0 K as substantiated by heat capacity, resistance, and magnetic measurements.

2. Experimental procedure

The samples were prepared from a stoichiometric mixture of Ni, graphite, and Th pieces (high purity). The constituent elements were placed together and melted in a Zr gettered arc furnace on a water-cooled Cu hearth under high purity argon. The sample was remelted five times to ensure good homogeneity. Due to the low vapor pressure of these constituent elements at melting temperature, the weight losses during arc melting were negligible (<0.5%). Some samples were annealed at 900 °C for two days and then quenched in liquid nitrogen. A microcomputer controlled diffractometer equipped with a copper target for Cu Kα (λ = 1.540 56 Å) radiation was used to get the powder x-ray diffraction patterns. The lattice parameters were determined by using the PowderCell software [19]. Magnetic data were obtained using a commercial VSM-SQUID by Quantum Design. The temperature dependence was obtained using a zero field cooling (ZFC) and field cooling (FC) process, using applied magnetic field at 10 Oe. After both ZFC and FC processes, the M versus H measurement was made at 1.8 K. Electrical resistivity measurements were made between 1.8 and 300 K using a conventional four-probe method. The samples were of irregular shape and fine gold wires were spot-welded to the sample and served as the voltage and current leads. These measurements were made with and without an applied magnetic field in order to estimate the upper critical field in a physical property measurement system (PPMS) machine. The specific heat of a piece cut from the sample

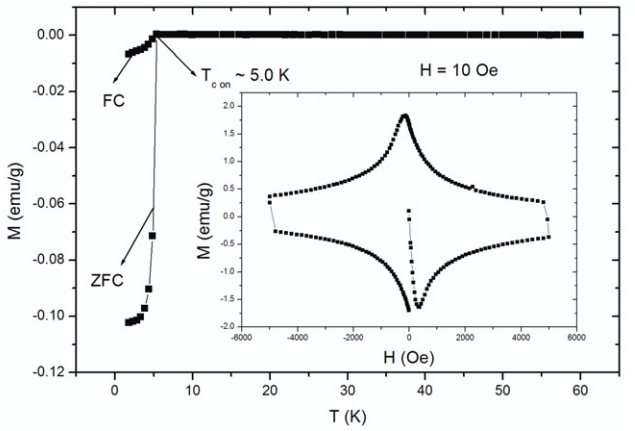

Figure 2. Magnetization as a function of temperature under ZFC and FC conditions at 10 Oe, displaying a clear superconducting transition close to 5.0 K. The inset displays the M versus H curve at a temperature of 1.8 K, where we observe a type II superconducting behavior.

was measured in the range of 0.4–10 K with a He^3 calorimeter in PPMS (Quantum Design) using the relaxation method. These measurements were carried out in applied magnetic field between 0 T $\leqslant B \leqslant$ 6.0 T.

3. Results and discussion

Figure 1 shows a comparison between experimental and simulated diffraction patterns. The simulation was carried by PowderCell software. The Miller indices have been omitted in order to avoid confusion when viewing the figure, due to the large number of peaks. There is excellent agreement between the two results, with an exception for minority peaks that can be indexed as a ThC_2 impurity, which is indicated by the * symbol. In the inset of this figure is shown the unit cell schematic of this compound. The Th atom is represented by a red sphere, Ni atom by a blue sphere and the black spheres represent carbon atoms. We do not observe any significant difference between as-cast and annealed samples. The refinement of the lattice parameter yields a = 13.92 Å, b = 7.14 Å, and c = 7.04 Å in excellent agreement with results reported in the literature [18]. The magnetization as a function of temperature in ZFC and FC regimes reveals a superconducting transition close to 5.0 K, as shown in figure 2. The difference between ZFC and FC strongly suggests type II superconductivity. The Meissner flux expulsion (FC) is about 7% of the diamagnetic flux expulsion, a characteristic of relatively strong pinning. This is confirmed by the M versus H data shown in the inset of figure 2. About 85% is the superconducting fraction estimated at 1.8 K, calculated from the linear behavior on the M versus H curve, again strongly suggesting bulk superconductivity. No significant variation of the superconducting behavior was observed in the as-cast and annealed samples, consistent with results obtained for x-ray diffraction. The extrapolation of the linear behavior in M versus H indicates a lower critical field at 1.8 K close to 80 Oe. This is a rough estimate because the demagnetization

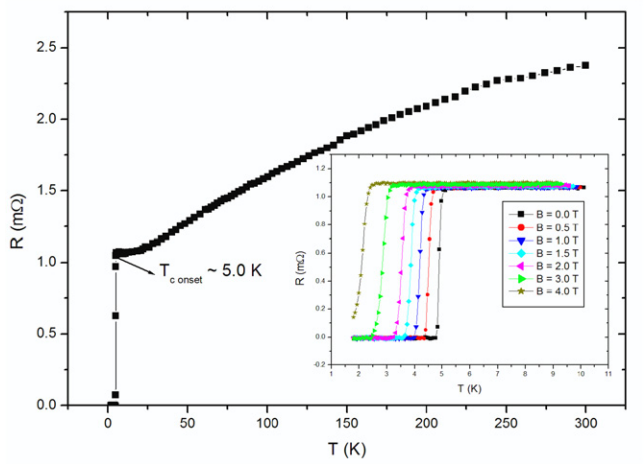

Figure 3. The resistance of $Th_3Ni_5C_5$ as a function of temperature at zero magnetic field. The inset shows a magnetoresistance for various applied magnetic fields in the 0 T $\leqslant \mu_o H \leqslant$ 4.0 T interval.

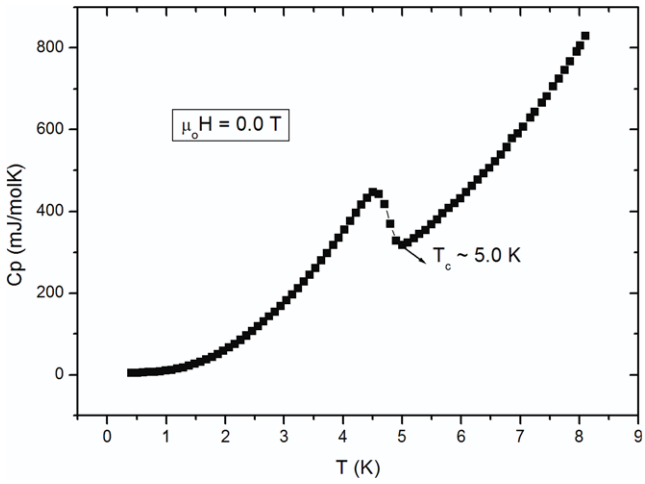

Figure 4. The heat capacity of the $Th_3Ni_5C_5$ polycrystalline sample between 0.4 and 9.0 K shows a clear superconducting transition at $T_c = 5.0$ K, consistent with figures 2 and 3 respectively.

factor was not taken into account, due to the irregular shape of the sample. Even if this lower critical field is not precise, it is possible to estimate the penetration depth (λ_L) through the relation $H_{c1} = \frac{\phi_o}{2\pi\lambda_L^2}$, where ϕ_o is a quantum flux equal to 2.068×10^{-15} T m^{-2}. The value estimated through this equation yields a penetration depth of $\lambda_L \sim 203$ nm.

Resistance data between 1.8 and 300 K for the polycrystalline $Th_3Ni_5C_5$ sample are presented in figure 3. The inset of this figure shows the magnetoresistance behavior. We are presenting resistance instead of resistivity because the irregular shape of the sample precludes accurately determining the geometrical factors. The onset superconducting critical temperature is close to 5.0 K in zero magnetic field, consistent with magnetic measurement (shown in figure 2). The sharp superconducting transition ($\Delta T_c \sim 0.2$ K), indicates good sample quality. Magnetoresistance as a function of temperature, shown in the inset, suggests a relatively high upper critical field (H_{c2}). These results are consistent

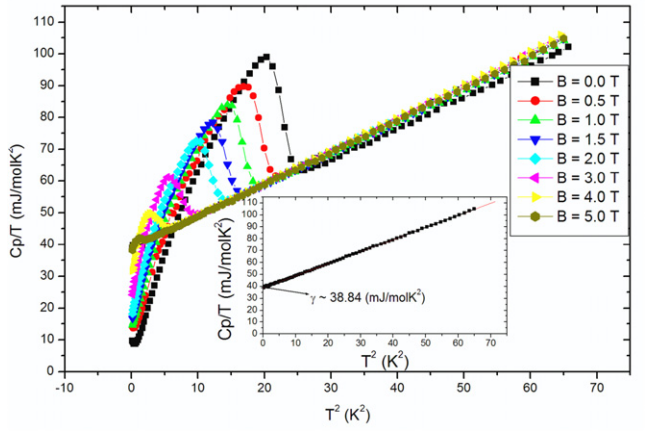

Figure 5. The Cp/T versus T^2 curve for several applied magnetic fields between 0 and $\mu_o H = 5.0$ T shows the shift of the superconducting critical temperature as a function of applied magnetic field, which is consistent with the electrical transport measurement shown in figure 3. The inset displays the behavior of Cp/T with T^2 under an applied magnetic field of $\mu_o H = 6.0$ T. The solid line is the fit of the experimental data to $c = \gamma T + \beta T^3$ between 0.4 and 8.0 K.

with the M versus T and M versus H curves, and also suggest bulk superconductivity. In order to confirm the bulk superconductivity of $Th_3Ni_5C_5$ we measured the heat capacity. An anomaly (jump) at 5.0 K is clearly observed in the temperature dependent heat capacity (C) measurement, shown in figure 4 with a temperature range of 0.4–8.0 K at zero magnetic field. This result is totally consistent with the M versus T and R versus T measurements, and represents clear evidence of bulk superconductivity in $Th_3Ni_5C_5$. Figure 5 shows the C/T against T^2 in various magnetic fields. The inset shows C/T against T^2 at $\mu_o H = 6.0$ T which reveals the normal state (C_n). The normal state specific heat can be fitted to the expression $C_n = \gamma T + \beta T^3$ by a least-square analysis, yielding the values $\gamma = 38.84$ mJ mol^{-1} K^{-2} and $\beta = 1.012$ mJ mol^{-1} K^{-4}. This β value corresponds to a Debye temperature of $\Theta_D \sim 293$ K and a Sommerfeld coefficient for the mole formula unit suggests a density of state at the Fermi level typical of transition metal superconductors. The subtraction of the phonon contribution allows us to evaluate the electronic contribution to the specific heat, plotted as C_e/T versus T in figure 6. An analysis of the jump yields $\Delta C_e/\gamma_n T_c \sim 1.1$ which is smaller than the weak-coupling Bardeen–Cooper–Schrieffer (BCS) prediction (1.43). Indeed, the specific heat C_s in the superconducting state shows marked deviations from conventional BCS theory as presented in figure 7. A great deviation can be observed at temperatures already close to T_c. The origin of these deviations in both figures is not obvious. On the other hand, we note that the C_e/T shows an unusual behavior at low temperature, i.e. an upturn for $T < 1.0$ K (figure 6). This upturn may be due to the magnetic Schottky contribution and/or the paramagnetism of unreacted Ni impurities. In fact, similar behavior was observed in MgB_2 where Fe impurities lead to an upturn in C/T at low temperature [20]. However, we cannot disregard the fact that this kind of behavior (like exponential behavior)

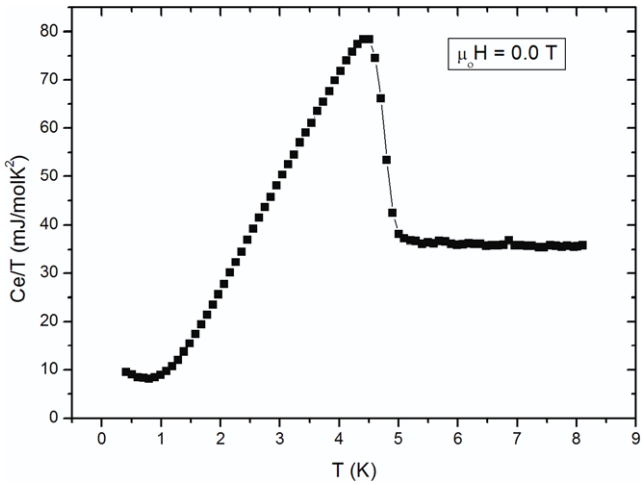

Figure 6. Temperature dependence of the electronic specific heat divided by temperature (C_e/T).

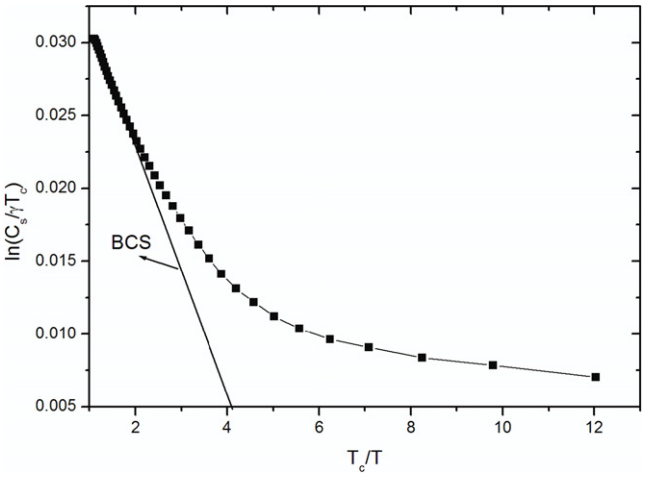

Figure 7. The C_s of the $Th_3Ni_5C_5$ polycrystalline sample in the superconducting state is plotted on a logarithmic scale versus T/T_c, showing a deviation from BCS behavior.

could also represent the possibility of a second gap in low temperature, due to the nodal structure in the Fermi surface. Indeed the possibility of a second gap is observed in MgB_2 due to the π band in the Fermi surface [21]. The presence of the impurity phase (ThC_2 as a minority phase) could be related to the deviation observed, but this kind of behavior can be observed in the annealed and as-cast sample and ThC_2 has no effect on the superconductivity [22]. The deviation from BCS ($\Delta C_e/\gamma_n T_c \sim 1.1$) would correspond to about 77% of the ideal value, but we estimate the impurity phase percentage ∼7% from the analyses of the powder x-ray diffraction pattern. This value is lower than the 23% from the analyses of the jump in specific heat. The deviation may be a real phenomenon in this material, but studies on phase pure material would be needed to determine this.

A comparison between the results shown in figures 3 and 5 shows excellent agreement. The shifts of the critical temperature as a function of applied magnetic field are consistent in both measurements. $\mu_o H_c$ and its temperature

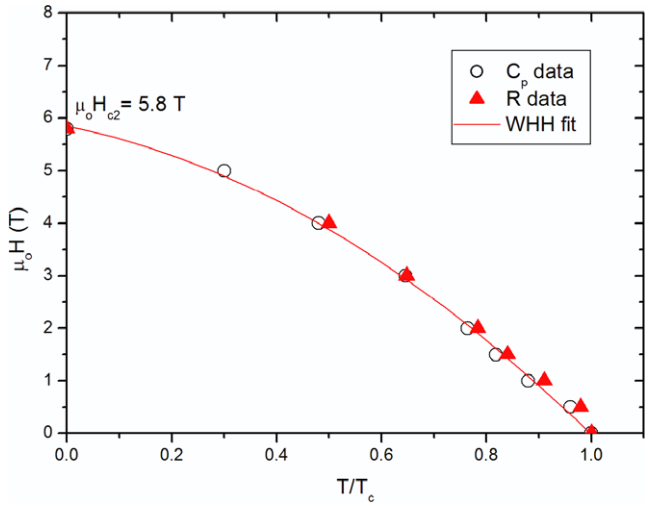

Figure 8. Temperature dependence of the upper critical field. Shown is a summary of the resistance and specific-heat measurements. The continuous line represents the WHH model.

dependence extracted from the figures allow an evaluation of the upper critical field at zero temperature. Figure 8 shows the $\mu_o H_c$ as a function of reduced temperature (T/T_c), extracted from both figures (figures 3 and 5). These results are in good agreement. The upper critical field at zero temperature ($\mu_o H_{c2(0)}$) can be estimated using the WHH formula [23] in the limit of short electronic mean free path (dirty limit),

$$\mu_o H_{c2}(0) = -0.693(\mathrm{d}H_{c2}/\mathrm{d}T)_{T=Tc} T_c.$$

Figure 8 shows the curve estimated by WHH which follows the data points very closely and gives a $\mu_o H_{c2}(0)$ value of 5.8 T. On the other hand, the spin–orbit scattering counteracts the effect of the Pauli paramagnetism, giving an upper bound to H_{c2} where the pair breaking is only induced by orbital fields. The temperature dependence of the upper critical field can either be explained by Pauli paramagnetism with extremely strong spin–orbit scattering or with a completely dominating orbital field effect. The Pauli limiting field is described by

$$\mu H^{\mathrm{Pauli}} = \frac{1.24 k_B T_c}{\mu_B}.$$

Within the same weak-coupling BCS theory this gives an upper critical field of 9.22 T, which is much higher than $\mu_o H_{c2}(0)$ in the absence of Pauli paramagnetism (5.8 T). Hence pair breaking in $Th_3Ni_5C_5$ is most probably determined by orbital fields.

The fitting of the figure 8 data allows an estimation of the coherence length, through the Ginzburg–Landau (GL) formula, $\mu_o H_{c2}(0) = \frac{\phi_o}{2\pi\xi_0^2}$, which yields $\xi_o \sim 75$ Å. At 1.8 K the coherence length is about 85 Å estimated from figure 8, whereas the penetration depth is about 207 nm. These values yield a GL $\kappa_{(1.8)} \sim 25$, which is much higher than $\frac{1}{\sqrt{2}}$. This κ is consistent with the behavior of a type II superconductor, as revealed by the M versus H curve (inset of figure 2).

Some nickel-rich compounds exhibit superconductivity, among them we can mention $MgCNi_3$ and $LnNi_2B_2C$ [24, 25].

The fact that superconducting compounds occur where so much Ni is present is always interesting, and $Th_3Ni_5C_5$ is a new example.

4. Conclusion

In summary, the excellent agreement of transition temperature as characterized by the magnetic, resistivity, and specific-heat data unambiguously indicates that $Th_3Ni_5C_5$ is a type II superconductor with $T_c \sim 5.0$ K. Our results presented in this paper disagree with the previous results which reported the discovery of the $Th_3Ni_5C_5$ organometallic phase where the authors claimed that this material was a simple Pauli paramagnet at low temperature [18].

Acknowledgments

We are grateful to Dr C Capan for assistance and use of the equipment. This work was supported by CNPq (Brazilian Agency grant no. 201455/2008-0), National Science Foundation NSF, and AFOSR MURI.

References

[1] Atoji M 1961 *J. Chem. Phys.* **35** 1950
[2] Atoji M and Medrud R 1959 *J. Chem. Phys.* **31** 332
[3] Hunt E 1951 *J. Am. Chem. Soc.* **73** 4777
[4] Zachariasen W H 1952 *Acta Crystallogr.* **5** 17
[5] Atoji M 1967 *J. Chem. Phys.* **46** 1891
[6] Stackelberg M V 1931 *Z. Elektrochem.* **37** 542
[7] Bowman A L, Krikorian N H, Arnold G P, Wallace T C and Nereson N G 1968 *Acta Crystallogr.* B **24** 1121
[8] Adachi G Y, Shibata Y, Ueno K and Shiokawa J 1976 *J. Inorg. Nucl. Chem.* **38** 1023
[9] Atoji M 1971 *J. Chem. Phys.* **54** 3504
[10] Atoji M 1972 *J. Chem. Phys.* **57** 2410
[11] Abache C and Oesterreicher H 1985 *J. Appl. Phys.* **57** 4112
[12] Pedziwiatr A T, Wallace W E and Burzo E 1986 *J. Magn. Magn. Mater.* **59** L179
[13] Gerse M H, Jeitschko W, Boonk L, Nientiedt J, Grobe J, Mörsen E and Leson A 1987 *J. Solid State Chem.* **70** 19
[14] Hoffmann R D and Jeitschko W 1986 *Z. Kristallogr.* **174** 85
[15] Nowotny H, Kieffer R, Benesovsky F and Laube E 1958 *Monatsh. Chem.* **89** 692
[16] King R B 1994 *Russ. Chem. Bull.* **43** 1285
[17] Lee W H, Zeng H K, Yao Y D and Chen Y Y 1996 *Physica* C **266** 138–42
[18] Moss M A and Jeitschko W 1991 *Z. Anorg. Allg. Chem.* **603** 57
[19] Kraus W and Nolze G 1996 *J. Appl. Crystallogr.* **29** 301
[20] Wang Y, Plackowski T and Junod A 2001 *Physica* C **355** 179
[21] Bouquet F, Fisher R A, Phillips N E, Hinks D G and Jorgensen J D 2001 *Phys. Rev. Lett.* **87** 047001
[22] Syu K J, Sung H H and Lee W H 2007 *Solid State Commun.* **141** 519
[23] Werthamer N R, Helfand E and Hohenberg P C 1966 *Phys. Rev.* **147** 295
[24] He T *et al* 2001 *Nature* **411** 54
[25] Cava R J *et al* 1994 *Nature* **367** 252